BiosyntheticSPAdes:
Reconstructing Biosynthetic Gene Clusters From Assembly Graphs
(Supplementary Material)

Dmitry Meleshko[1,2], Hosein Mohimani[3,4], Vittorio Tracanna[5],
Iman Hajirasouliha[6,7], Marnix H. Medema[5], Anton Korobeynikov[1,8],
Pavel A. Pevzner[1,3,*]

[1]Center for Algorithmic Biotechnology, Institute for Translational Biomedicine,
St. Petersburg State University, St. Petersburg, Russia
[2]Tri-Institutional PhD Program in Computational Biology and Medicine,
Weill Cornell Medical College, New York, United States
[3]Department of Computer Science and Engineering, University of California, San Diego,
[4]Computational Biology Department, School of Computer Sciences,
Carnegie Mellon University
[5]Bioinformatics Group, Wageningen University, Wageningen, The Netherlands

[6]Institute for Computational Biomedicine, Department of Physiology and Biophysics,
Weill Cornell Medicine of Cornell University, New York, United States
[7]Englander Institute for Precision Medicine, Meyer Cancer Center,
Weill Cornell Medicine, New York, United States
[8]Department of Statistical Modelling, St. Petersburg State University, St. Petersburg, Russia
*Corresponding author, ppevzner@ucsd.edu

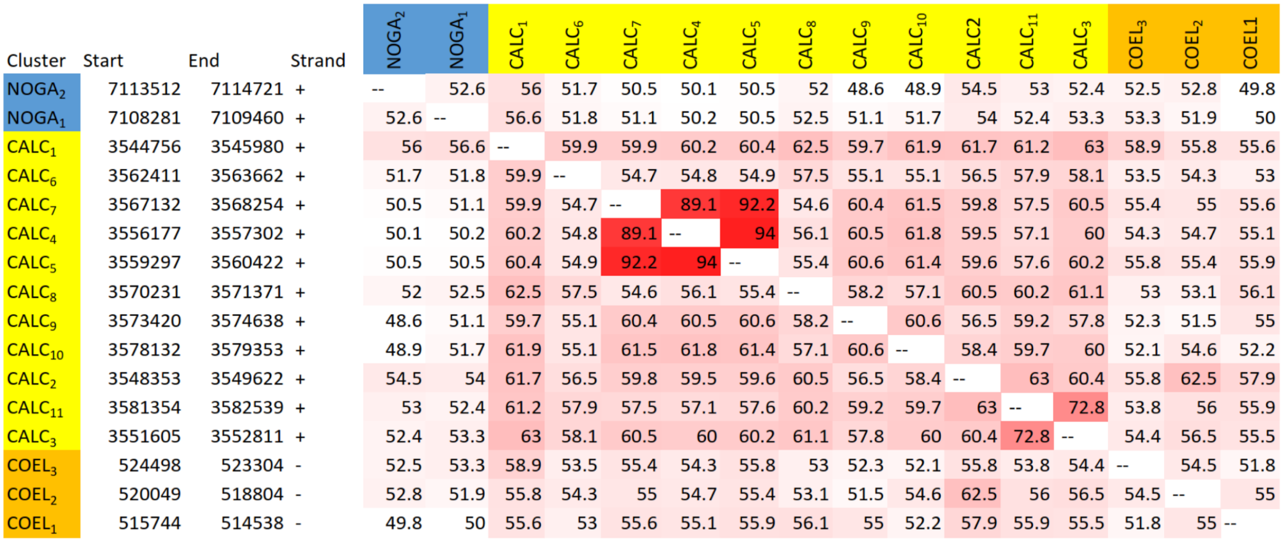

Cluster	Start	End	Strand	NOGA$_2$	NOGA$_1$	CALC$_1$	CALC$_6$	CALC$_7$	CALC$_4$	CALC$_5$	CALC$_8$	CALC$_9$	CALC$_{10}$	CALC2	CALC$_{11}$	CALC$_3$	COEL$_3$	COEL$_2$	COEL1
NOGA$_2$	7113512	7114721	+	--	52.6	56	51.7	50.5	50.1	50.5	52	48.6	48.9	54.5	53	52.4	52.5	52.8	49.8
NOGA$_1$	7108281	7109460	+	52.6	--	56.6	51.8	51.1	50.2	50.5	52.5	51.1	51.7	54	52.4	53.3	53.3	51.9	50
CALC$_1$	3544756	3545980	+	56	56.6	--	59.9	59.9	60.2	60.4	62.5	59.7	61.9	61.7	61.2	63	58.9	55.8	55.6
CALC$_6$	3562411	3563662	+	51.7	51.8	59.9	--	54.7	54.8	54.9	57.5	55.1	55.1	56.5	57.9	58.1	53.5	54.3	53
CALC$_7$	3567132	3568254	+	50.5	51.1	59.9	54.7	--	89.1	92.2	54.6	60.4	61.5	59.8	57.5	60.5	55.4	55	55.6
CALC$_4$	3556177	3557302	+	50.1	50.2	60.2	54.8	89.1	--	94	56.1	60.5	61.8	59.5	57.1	60	54.3	54.7	55.1
CALC$_5$	3559297	3560422	+	50.5	50.5	60.4	54.9	92.2	94	--	55.4	60.6	61.4	59.6	57.6	60.2	55.8	55.4	55.9
CALC$_8$	3570231	3571371	+	52	52.5	62.5	57.5	54.6	56.1	55.4	--	58.2	57.1	60.5	60.2	61.1	53	53.1	56.1
CALC$_9$	3573420	3574638	+	48.6	51.1	59.7	55.1	60.4	60.5	60.6	58.2	--	60.6	56.5	59.2	57.8	52.3	51.5	55
CALC$_{10}$	3578132	3579353	+	48.9	51.7	61.9	55.1	61.5	61.8	61.4	57.1	60.6	--	58.4	59.7	60	52.1	54.6	52.2
CALC$_2$	3548353	3549622	+	54.5	54	61.7	56.5	59.8	59.5	59.6	60.5	56.5	58.4	--	63	60.4	55.8	62.5	57.9
CALC$_{11}$	3581354	3582539	+	53	52.4	61.2	57.9	57.5	57.1	57.6	60.2	59.2	59.7	63	--	72.8	53.8	56	55.9
CALC$_3$	3551605	3552811	+	52.4	53.3	63	58.1	60.5	60	60.2	61.1	57.8	60	60.4	72.8	--	54.4	56.5	55.5
COEL$_3$	524498	523304	-	52.5	53.3	58.9	53.5	55.4	54.3	55.8	53	52.3	52.1	55.8	53.8	54.4	--	54.5	51.8
COEL$_2$	520049	518804	-	52.8	51.9	55.8	54.3	55	54.7	55.4	53.1	51.5	54.6	62.5	56	56.5	54.5	--	55
COEL$_1$	515744	514538	-	49.8	50	55.6	53	55.6	55.1	55.9	56.1	55	52.2	57.9	55.9	55.5	51.8	55	--

Supplementary Figure S1: The percent identity matrix for A-domains in three BGCs in *S. coelicolor A3(2)*. A-domains CALC$_4$, CALC$_5$, CALC$_7$ (numbers denotes index in the CALC BGC sequence) in the CALC gene cluster (shown as red entries) share identical segments of 96 nucleotides or longer.

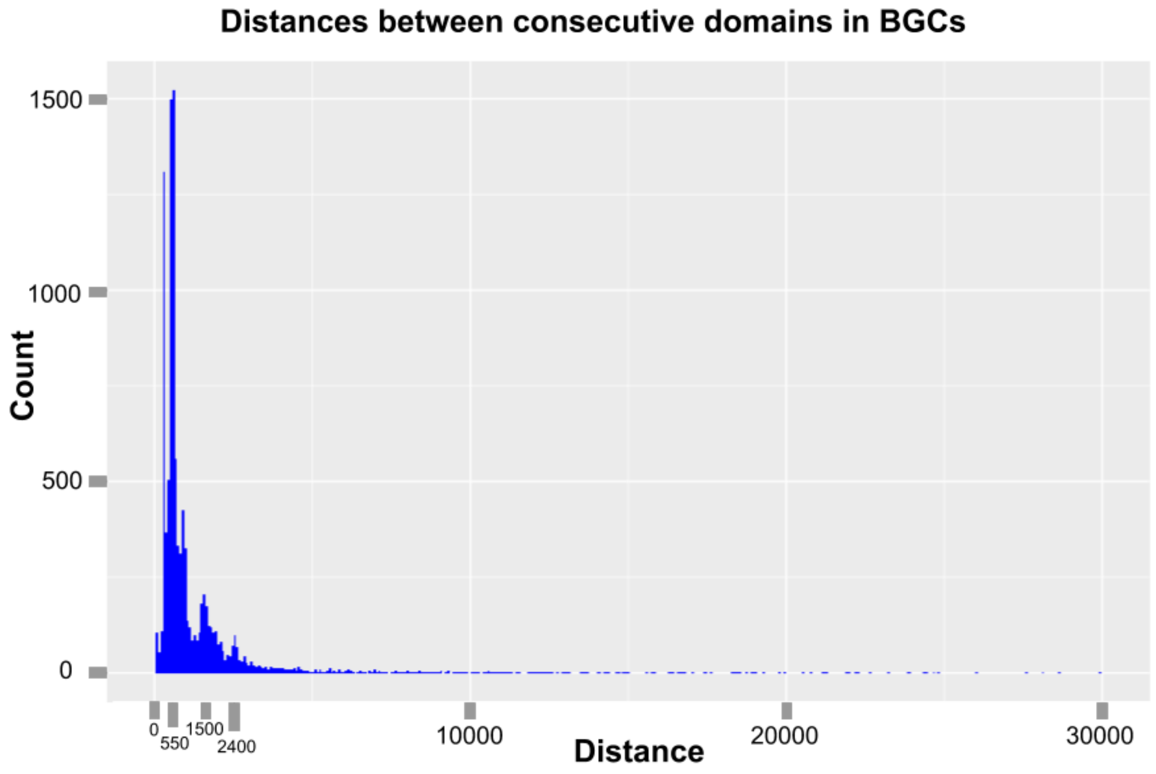

Supplementary Figure S2. Histogram of distances between consecutive domains in NRP and PK BGCs from the MIBIG database. The distances are computed for A, C, TE, AT, KS and KR domains.

#edges in the assembly graph	1	2	3	4	5	6	7	8	9	≥10
#genes	7625	112	90	23	35	5	10	1	1	8
median gene length	849	855	843	1443	1158	1020	1422	1011	2889	1656

Supplementary Table S1. Number of genes in S. coelicolor A3(2) categorized by the number of edges they traverse in the SPAdes assembly graph (total of 7910 genes). Even after repeat resolution in the assembly graph using exSPAnder, 54 genes in the S. coelicolor genome remain split over multiple scaffolds.

locus ID	Gene	gene length
SCO6275	**type I polyketide synthase**	**13674**
SCO3231	**CDA peptide synthetase II**	**11013**
SCO0492	**peptide synthetase**	**10932**
SCO6274	**type I polyketide synthase**	**10731**
SCO3232	**CDA peptide synthetase III**	**7254**
SCO6827	**polyketide synthase**	**7077**
SCO6428	hypothetical protein	6945
SCO5892	**polyketide synthase**	**6894**
SCO0127	**beta keto-acyl synthase**	**6723**
SCO7682	**non-ribosomal peptide synthase**	**6690**
SCO6220	hypothetical protein	6552
SCO6273	**type I polyketide synthase**	**6459**
SCO0126	**beta keto-acyl synthase**	**6249**
SCO7683	**non-ribosomal peptide synthase**	**5529**
SCO5748	sensory histidine kinase	5490
SCO2226	bifunctional alpha-amylase/dextrinase	5397
SCO3285	large glycine/alanine rich protein	5319
SCO1182	hypothetical protein	5181
SCO5761	ATP-dependent DNA helicase	5073
SCO6687	DNA-binding protein	5037
SCO3869	WD-40 repeat-containing protein	5031
SCO2999	hypothetical protein	4962
SCO6626	protein kinase	4674
SCO1407	hypothetical protein	4662
SCO2383	hypothetical protein	4638
SCO4508	cell division-like protein	4578
SCO2026	**glutamate synthase**	**4545**
SCO2499	transport ATPase	4419
SCO4009	bifunctional histidine kinase and regulator	4392
SCO7015	glycosyl hydrolase	4302
SCO6432	**peptide synthase**	**4224**
SCO5710	large Pro/Ala/Gly-rich protein	4101
SCO6348	hypothetical protein	4086
SCO2450	Ser/Thr protein kinase (regulator)	4050

SCO2975	hypothetical protein	4038
SCO2599	hypothetical protein	4023
SCO2259	multidomain-containing protein family	4005
SCO7327	two-component system sensory histidine kinase	3996
SCO5544	hypothetical protein	3990
SCO4092	ATP-dependent helicase	3984
SCO5397	large Ala/Glu-rich protein	3981
SCO5734	ATP/GTP binding protein membrane protein	3966
SCO1184	hypothetical protein	3963
SCO6457	beta-galactosidase	3924
SCO4655	DNA-directed RNA polymerase subunit beta'	3900
SCO6635	bacteriophage resistance gene pglY	3885
kgd	alpha-ketoglutarate decarboxylase	3819
SCO6004	ATP/GTP binding protein	3807
SCO3033	integral membrane regulatory protein	3807
SCO6219	Ser/Thr protein kinase	3786
SCO7176	peptidase	3762
SCO4263	transcriptional regulator	3756
SCO0432	peptidase	3738
SCO2763	ABC transporter ATP-binding protein	3732
SCO7188	peptidase	3720
SCO6572	glycosyl hydrolase	3717
SCO0216	nitrate reductase subunit alpha NarG2	3702
SCO6535	nitrate reductase subunit alpha NarG	3696
SCO4947	nitrate reductase subunit alpha NarG3	3684
SCO5184	ATP-dependent DNA helicase	3669
SCO2446	peptidase	3663
cobN	cobaltochelatase subunit CobN	3654
SCO1554	nicotinate-nucleotide-dimethylbenzimidazole phosphoribosyltransferase	3639
SCO6627	hypothetical protein	3633
SCO5331	DNA methylase	3603
SCO2590	glycosyltransferase	3594
SCO5577	chromosome associated protein	3561

SCO1739	DNA polymerase III subunit alpha	3558
SCO3109	transcriptional-repair coupling factor	3555
dnaE	DNA polymerase III subunit alpha	3540
SCO3947	ABC transporter	3519
SCO6688	hypothetical protein	3516
SCO6431	**peptide synthase**	**3516**
SCO3168	protease	3516
SCO1657	**methionine synthase**	**3513**
SCO4969	regulatory protein	3504
rpoB	DNA-directed RNA polymerase subunit beta	3486
SCO5183	ATP-dependent DNA helicase	3480
SCO6198	hypothetical protein	3471
SCO5280	ATP-binding protein	3447
SCO6593	hypothetical protein	3444
SCO0488	hydrolase	3417
SCO0370	DNA-binding protein	3405
SCO7037	hypothetical protein	3396
SCO0546	pyruvate carboxylase	3375
SCO0072	hypothetical protein	3354
SCO4116	AfsR-like regulatory protein	3345
SCO2672	hypothetical protein	3342
SCO5540	hypothetical protein	3336
SCO4250	hypothetical protein	3336
SCO5511	membrane associated phophodiesterase	3327
carB	**carbamoyl phosphate synthase large subunit**	**3309**
SCO2637	serine protease	3297
SCO5271	hypothetical protein	3291
SCO5506	regulatory protein	3276
SCO3542	integral membrane protein with kinase activity	3270
SCO6994	hypothetical protein	3261
SCO0369	hypothetical protein	3258
SCO5717	hypothetical protein	3252
SCO2549	Protease	3204

Supplementary Table S2. List of 100 longest genes in the Streptomyces coelicolor A3(2) genome. Genes forming BGC genes are shown in bold.

locus ID	gene	gene length	#contigs
SCO6274	**type I polyketide synthase**	**13674**	**9**
SCO6273	**type I polyketide synthase**	**10731**	**7**
SCO3232	**CDA peptide synthetase III**	**7254**	**2**
SCO6270	oxidoreductase alpha-subunit	6457	2
SCO2599	hypothetical protein	4021	2
SCO6836	transcription regulator ArsR	3994	2
SCO5540	hypothetical protein	3334	2
SCO2000	ATP-binding RNA helicase	2997	2
SCO6789	fatty oxidation protein	2202	2
SCO6275	**type I polyketide synthase**	**2159**	**3**
SCO6082	glycogen debranching protein	2107	2
SCO5443	alpha-amylase	2026	3
SCO7327	two-component system sensory histidine kinase	2008	2
SCO4595	Oxidoreductase	1936	2
SCO4777	protein Ser/Thr kinase	1800	2
SCO6661	glucose-6-phosphate 1-dehydrogenase	1777	4
SCO6659	glucose-6-phosphate isomerase	1651	3
SCO4296	chaperonin GroEL	1626	2
SCO4762	chaperonin GroEL	1626	2
SCO6832	methylmalonyll-CoA mutase	1596	3
SCO4258	hydrolytic protein	1458	2
SCO4257	hydrolytic protein	1443	2
SCO5087	actinorhodin polyketide beta-ketoacyl synthase subunit alpha	1404	2
SCO2931	ABC transporter ATP-binding protein	1275	2
SCO5393	ABC transporter ATP-binding protein	1270	2
SCO2366	hypothetical protein	1141	3
SCO6837	arsenic resistance membrane transport protein	1107	2
SCO4594	2-oxoglutarate ferredoxin oxidoreductase subunit beta	1057	2
SCO6269	2-oxoglutarate ferredoxin oxidoreductase subunit beta	1051	2
SCO4885	lipoprotein	1047	2
SCO1471	transposase	1020	3
SCO2632	transposase	1020	4
SCO4370	transposase	1020	3
SCO4698	IS1652 transposase	1020	3
SCO4183	transposase	1018	3

SCO5514	ketol-acid reductoisomerase	999	3
SCO0091	IS1652 transposase	957	2
SCO0368	transposase	957	2
SCO7335	alpha-amylase	957	3
SCO7803	insertion element transposase	957	2
SCO5641	transposase	955	2
SCO7819	hypothetical protein	847	2
SCO5634	pseudo	596	2
SCO5292	ATP/GTP-binding protein	576	2
SCO4061	hypothetical protein	556	2
SCO6395	pseudo	379	3
SCO7805	hypothetical protein	336	2
SCO6403	hypothetical protein	309	2
SCOr15	5S ribosomal RNA	121	2
SCOr04	5S ribosomal RNA	119	2
SCOr01	5S ribosomal RNA	118	2
SCOr10	5S ribosomal RNA	117	2
SCOt05	tRNA	72	2
SCOt07	tRNA	72	2

Supplementary Table S3. The list of 54 genes from Streptomyces coelicolor A3(2) that span multiple contigs even after repeat resolution in the SPAdes assembly graph. The length of genes in this table varies from 72 to 13762 (average length is 2997 nucleotides). Multiple biosynthetic genes (e.g., the genes encoding the calcium-dependent antibiotic) are split over several contigs (shown in bold). Note that in addition to NRPSs and PKSs, other long genes including 16S RNA genes are also highly fragmented in metagenomic assemblies.

Appendix A: Coupling biosyntheticSPAdes and NRPquest for PNP reconstruction

Each of the rural postman routes generated by biosyntheticSPAdes corresponds to a sequence of A-domains and thus allows one to generate putative NRPs encoded by this sequence using *nonribosomal code* (Stachelhaus and Marahiel 1999). Tandem mass spectra can be matched against these putative NRPs resulting in *Peptide-Spectrum Matches* (*PSMs*) with varying P-values (Mohimani and Pevzner, 2016). A PSM with the lowest P-value reveals the NRP (and thus the rural postman tour) that is more likely to be correct than others.

To demonstrate how this approach works, we matched both putative CALC BGCs (corresponding to two rural postman routes for the CALC BGC) against a high resolution mass spectral dataset from *S. coelicolor* deposited in the Global Natural Products Social (GNPS) molecular network (Wang et al. 2016) with MassiveID MSV000078839 (total of 11952 spectra). For each A-domain, we analyzed the top three candidate amino acids predicted by NRPSPredictor2, and considered linear, cyclic, and branch-cyclic structures. This resulted in 20720 candidate structures for each sequence, and we searched all those structures against all mass spectra of *S. coelicolor* using Dereplicator (Mohimani et al. 2017), allowing for a single blind modification. The correct sequence resulted in a score 16 (P-value $8.7 * 10^{-15}$), while the incorrect sequence resulted in a score 15 (P-value $2.9 * 10^{-14}$). This illustrates that coupling of biosyntheticSPAdes with peptidogenomics leads to elucidation of NRPs encoded by predicted NRP BGCs.

Appendix B: biosyntheticSPAdes output format

BiosyntheticSPAdes stores all output files in a user-specified folder.

- <output_dir>/orderings.fasta contains putative sequences for all putative BGCs in the fasta format. Every header of a fasta record has the following format:

  >NODE_1_length_60699_cluster_3_candidate_2

  Here 1 is the identifier of the BGC sequence, 60699 is its length in nucleotides, 3 is the number of BGC subgraph that generated this sequence, and 2 is the number of rural postman routes generated from this subraph. We output at most 50 putative paths for each BGC subgraph according to their order in the Depth First Search traversal.
- <output_dir>/bgc_in_gfa/ folder contains the GFA file for each BGC subgraph. These files contain the assembly graph structures and can be visualized with tools such as Bandage (Wick et al. 2015)
- <output_dir>/bgc_statistics.txt contains information about each BGC subgraph and each rural postman route generated from this subgraph. For the BGC subgraph, it shows the number of

domains, the number of strong and weak edges in the corresponding scaffolding graph, and the predicted BGC type (PK, NRP, PK/NRP, or not known). For each rural postman route, it shows an arrangement of domains and positions of domains on putative BGC sequence.

Appendix C: Putative NRP BGCs in the CYANO dataset

The CYANO dataset proved to be a rich source of natural products (Kleigrewe et al. 2015, Boudreau et al. 2015, Cummings et al. 2016). It is also a difficult test for the biosyntheticSPAdes algorithm for the following three reasons:

- Although the heterotrophic bacterial contaminants in this dataset encode some BGCs, these BGCs are difficult to reconstruct due to the low depth of coverage. E.g., biosyntheticSPAdes identified three NRP synthetases (108 kb, 44 kb, and 43 kb in length) with low mean coverage 8X arising from some low-abundance bacteria.
- Since some BGCs are located in close proximity to each other in the assembly graph, a single BGC subgraph and corresponding scaffolding graph may contain domains from several BGCs, thus preventing the rural postman approach from finding feasible routes (Supplementary Figure S3). Reconstruction of BGCs from such BGC subgraphs is challenging since they often span complex repeat structures. For example. biosyntheticSPAdes identified a BGC subgraph with more than 200 domains in the CYANO dataset. Such BGC subgraphs may encode dozens of BGCs.
- Many BGCs have highly similar domains resulting in domain collapsing. To perform domain restoration, one has to estimate how many domains were collapsed on a single edge in the assembly graph, which becomes challenging due to variations in the coverage depth.

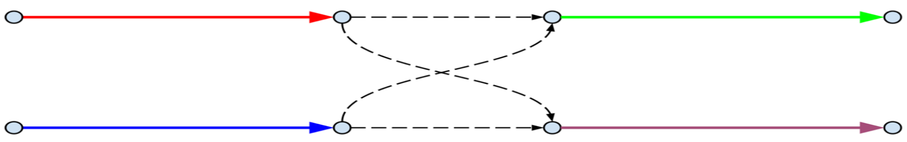

Supplementary Figure S3. An example of the scaffolding graph without a rural postman route. This scaffolding graph is likely formed by two BGCs.

Despite the fact, that biosyntheticSPAdes faced all three challenges analyzing the CYANO dataset, it reconstructed five putative NRP synthetases with complexities 20, 9, 5, 5, and 2, respectively. Our analysis revealed that the CYANO sample contains novel BGCs that fell under the radar of previous studies (based on extensive manual curation) but were reconstructed by biosyntheticSPAdes.

The BGCs with complexities 20 and 9 likely originated from the low-coverage contaminant bacteria and their BGC subgraphs include multiple isolated edges. SPAdes/metaSPAdes combined them into a single scaffold but the nucleotide sequence of this scaffold contains stretches of Ns, making it difficult to infer the nucleotide sequences of the domains. Another possibility is that these two putative NRP synthetases represent parts of a single NRP that was not assembled into a single contig by SPAdes/metaSPAdes. Although two BGCs with multiplicity five have complex BGC subgraphs with loops and long repeats, (Supplementary Figure S4), there exist single rural postman routes in their scaffolding graphs. Since AntiSMASH analysis did not reveal any similarities with known BGCs, they likely represent novel NRP synthetases. The NRP synthetase with complexity 2 has a simple graph structure (all domains lie on a single edge of the assembly graph) and is similar to the known aeruginoside BGC (52% gene similarity and consistent gene order).

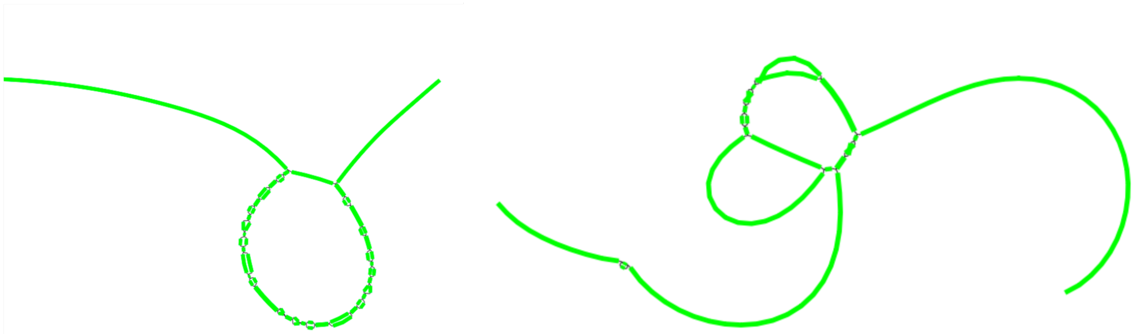

Supplementary Figure S4. Two complex BGC subgraphs from the CYANO dataset visualized with the Bandage tool (Wick et al. 2015). Grey edges represent edges of the assembly graph and each union of connected black edges represents a vertex of the assembly graph.

Appendix D: Biosynthetic capacity of the HMP datasets

	dataset ID	total length of long contigs (Mb)	N50 (kb)	#A-domains	#AT-domains	# A/AT-domains per 1 Mb	# BGC subgraphs with complexity 1-3	# BGC subgraphs with complexity 4-6	# BGC subgraphs with complexity ≥7
Keratinized gingiva	019125	50.5	44,0	57	24	1.60	12	0	0
	014473	41.2	6,2	60	36	2.33	15	0	0
	015060	47.3	3,8	61	50	2.34	18	1	0
Buccal mucosa	018443	129.5	3,6	166	83	1.92	47	1	0
	023930	29.3	12,1	41	19	2.05	10	0	0
Stool	052697	211.0	12,3	287	85	1.76	74	0	0
	011239	136.2	8,4	215	48	1.93	45	0	0
	016335	189,5	7,0	268	62	1.69	51	0	0
Gingivival plaque	013950	95.8	4,0	142	72	2.23	40	0	0
	063215	76.7	3,3	169	52	2.88	26	4	0
	019029	112.8	2,6	147	76	1.98	28	2	0
Subpravingal plaque	013723	149.0	3,4	242	117	2.41	59	7	0
	015574	149.3	3,3	258	104	2.42	67	7	1
	049318	221.2	3,9	300	124	1.92	80	3	0
Tongue dorsum	050244	174.3	5,8	204	83	1.65	47	4	0
	024081	144.0	8,5	176	66	1.68	47	3	0
	015762	168.3	6,3	208	85	1.74	57	3	0
Throat	019127	91.6	4,6	136	46	1.97	34	0	0
	019027	76,4	4,2	90	40	1.70	23	1	0
	014689	63,2	4,1	76	38	1.80	17	1	0

Supplementary Table S4: Statistics of A-domains and AT-domains in various samples from the HMP dataset. Long contigs are defined as contigs longer than 1 kb. Dataset identifier is the numerical part of the SRX accession id.

Appendix E: Putative NRP synthetases in the subpravingal plaque samples from the HMP dataset

Subpravingal plaque samples from the HMP dataset contain more nontrivial BGCs as compared to the samples from other human body sites. biosyntheticSPAdes identified 18 non-trivial BGC subgraphs in three subpravingal plaque datasets, including (i) 5 BGCs with high-coverage edges, (ii) 10 BGCs without repetitive regions but with coverage gaps, and (iii) 3 BGCs with coverage gaps and complex BGC subgraphs. Supplementary Figure S5 provides examples of two BGC subgraphs from categories (ii) and (iii).

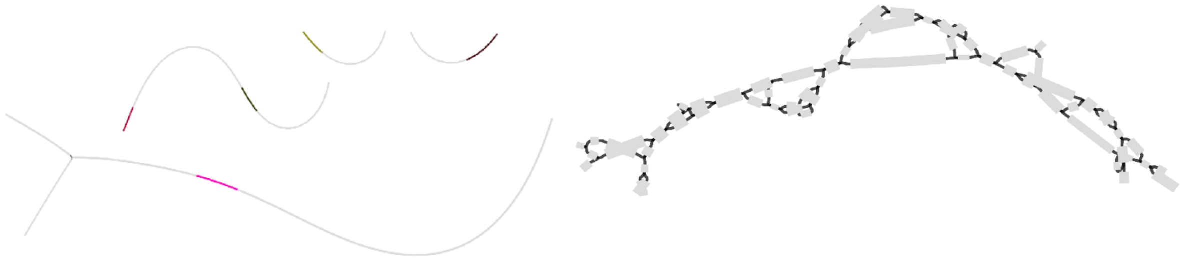

Supplementary Figure S5. Two low coverage BGC subgraphs from subpravingal plaque samples from the HMP dataset. Both subgraphs were visualized using Bandage tool (Wick et al. 2015). Grey edges represent edges of the assembly graph and each union of connected black edges represents a vertex of the assembly graph. (Left) A BGC subgraph for a low coverage region with coverage gaps. A and AT-domains are shown by different colors. (Right) A fragment of a BGC subgraph with low coverage and complex repeat structure. Each non-repetitive edge has coverage between 3X and 5X. This fragment of the assembly graph contains at least three AT-domains but none of them was assembled into a single contig. As the result, only parts of these domains were identified by HMMer. Corresponding scaffolding graph for this BGC subgraph doesn't contain any rural postman routes.

The assembly graph in category (ii) are simple but their nucleotide sequences are incomplete with many gaps (represented as multiple stretches of Ns). These gaps lead to difficulties in the cases when the domain sequence falls into the gaps. Also, it is not clear how to determine whether a reconstructed putative BGC is complete in the case of low coverage. For example, if the first and the last domains are located near the end of the putative sequence of the BGC, it is not clear whether the BGC is complete as some of its domains can be located in another BGC subgraph.

In contrast, biosyntheticSPAdes recovered all BGC with high coverage, including the one with a complex repeat structure analyzed in the main text (Supplementary Table S5)

BGC subgraph	predicted type	# domains	# rural postman routes	domain arrangement

1	NRPS	14	2	TE-TE-A-C-A-C-A-C-A-C-A-C-A-C TE-TE-A-C-A-C-A-C-A-C-A-C-A-C
2	NRPS/PKS	12	1	C-A-KS-AT-C-A-KS-C-A-KS-TE-KS
3	NRPS	18	1	A-C-A-C-A-C-A-C-A-C-A-C-A-C-A-C-TE-TE
4	NRPS/PKS	13	1	KS-AT-KR-TE-C-A-C-C-KS-AT-KR-C-A
5	NRPS/PKS	10	1	A-C-A-KS-AT-C-A-C-TE-TE

Supplementary Table S5. Statistics of five putative BGCs from the subpravingal plaque datasets with high coverage depth.

Appendix F: Reference-based putative BGC ranking algorithm

If biosyntheticSPAdes outputs several putative BGCs (*pBGCs*) for a single BGC gene cluster, it is not clear which of them is correct. In such cases, biosyntheticSPAdes uses a BGC ranking algorithm to compare each putative BGC against all reference BGCs (rBGCs) from a database of all BGCs from the reference genome sequences, and report the pair of pBGC and rBGC that are most similar to each other.

First, the order and positions of all domains in a pBGCs and all reference rBGCs are predicted with antiSMASH. For each pBGC-rBGC pair, biosynthetiSPAdes constructs a bipartite graph, where nodes are domains and edges connect a domain in pBGC with a domain rBGC if both these domains have the same type, e.g., A-domains. The edge weight is defined as the amino acid sequence similarity for the corresponding domain pair. biosynthetiSPAdes further computes the *maximum-weight matching* in the constructed bipartite graph using the Hungarian algorithm (Kuhn et al., 1955) (Supplementary Figure S6). The matching nodes in the maximum-weight matching are referred to as the *domain twins*.

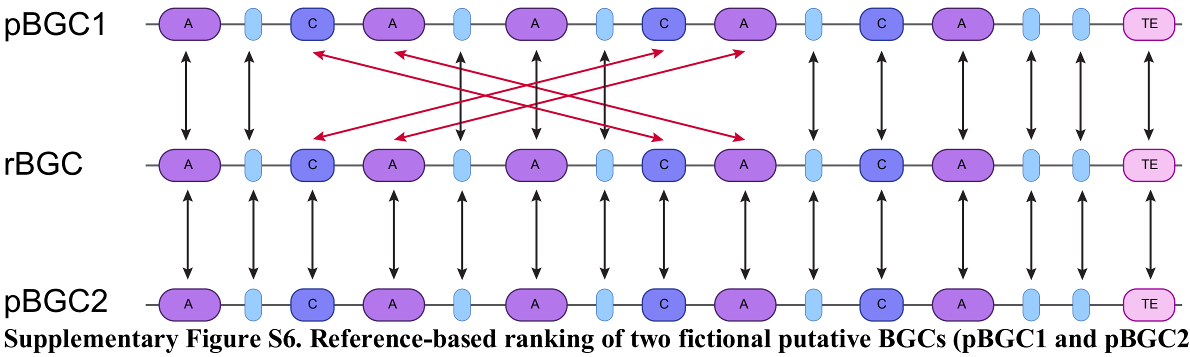

Supplementary Figure S6. Reference-based ranking of two fictional putative BGCs (pBGC1 and pBGC2) according to their similarity to an rBGC in the antiSMASH-DB database. To find which of two pBGC has a better match with the rBGC, the Hungarian algorithm determines domain twins between each pBGCs and the rBGC. Black and red arrows connect twin domains, red arrows further connect twin domains which will lower the score between rBGC and pBCG1 as the domain order in pBGC1 does not match the reference.

The closest rBCG from the database is taken based on the *Domain Sequence Similarity* (*DSS*) score described below.

The similarity score between two BGC clusters should take into account the sequence similarity, the domain composition, and the ordering of the domains. We also use a concept of highly similar domains – *domain twins* to find sequence similarity only between relevant domains of BGCs. We find a set of domain twins of a pBGC and rBGC as follows:

1) Construct a bipartite graph $G = (U, V, E)$, where U is the set of nodes that correspond to the domains of the first BGC, V is the set of nodes that correspond to the domains of the second BGC, and E is the set of edges that connecting pairs of domains from *U* and *V* of the same type (e.g. A-domains, C-domains, etc.)
2) Compute the similarity score between all pairs of domains of the same type as the amino acid sequence identity of their alignment. The weight of the edge between two domains in the bipartite graph is defined as the similarity score between these domains.
3) Find the maximum weight matching in the bipartite bipartite graph using the Hungarian algorithm (Kuhn, H. W., 1955). Pairs of domains connected by an edge from the maximum weight matching are called the *domain twins*.

To find a best matching pBGC-rBGC pair, we define the Domain Sequence Similarity (DSS) score. The DSS score is a measure of similarity between the amino acid sequences of twin domains between two BGCs. DSS also penalizes for domains that have no twin or different ordering of twin domains.

Let M be the subset of edges in the maximum weight matching for anrBGC-pBGC Pair, and *DT* be a set of *domain types* (e.g. A-domains, C-domains, etc.). Given a BGC, we refer to the number of domains of the specific *type* in this BGC $N^{type}(BGC)$. Given the order of the twin domains in an rBGC $(r_1, r_2, \ldots, r_{|M|})$ and a pBGC $(p_1, p_2, \ldots, p_{|M|})$, we analyze all domain twins (r_i, p_j) and (r_k, p_l) and classify a pair as an *inversion* if $k > i$ and $j > l$. We define the *inversion index* $I(rBGC, pBGC)$ as the total number of inversions between an *rBGC* and a *pBGC* divided by the$\binom{M}{2}$, the maximum possible number of inversions between two permuatations of length |*M*|. Given an rBGC-pBGC Pair (*rBGC, pBGC*) we define its *Domain Sequence Similarity* score *DSS*(*rBGC, pBGC*) as follows:

$$DSS(rBGC, pBGC) = \sum_{type \in DT} \frac{\sum_{e \in M_{type}} weight(e)}{\max\left(N^{type}(rBGC), N^{type}(pBGC)\right)} (1 - I(rBGC, pBCG\ ))$$

where M_{type} is the subset of edges of the given *type* in the maximum weight matching and $weight(e)$ is the weight of an edge e in the bipartite graph. Note that the DSS score penalizes domains that do not participate in twin pairs.

Given a set of putative BGCs and a set of reference BGCs, biosyntheticSPAdes selects an rBGC-pBGC Pair with the maximum DSS score and outputs the pBGC from this pair as the most likely solution.

Appendix G: Ranking putative BGCs from *Streptomyces coelicolor* A3(2) and *Streptomyces avermitilis* MA-4680

biosyntheticSPAdes assembly of the calcium dependent antibiotic (CALC) NRPS in *S. Coelicolor* produced two putative BGCs that we refer to as CALC_1 and CALC_2. These two putative BGCs were scored against all BGCs in antiSMASH-DB (excluding CALC itself) to identify which putative BGC is the most similar to known BGCs. To illustrate our approach, we analyzed an rBGC with the highest DSS scores against both CALC_1 and CALC_2: calcium dependent antibiotic BGC from *Streptomyces lividans* TK24. The rBGC chosen using the DSS score belong to the same genus suggesting that the concept of the DSS score helps to identify the correct domain order.

Since the MiBIG database contains the CALC BGC from *S. Coelicolor A3(2)* database, it was possible to also compare the two putative BGCs to their annotated version in MiBIG. Table S6 and Figure S6 illustrate that CALC_2 has higher domain order consistency and achieves higher DSS score with both the rBGC from antiSMASH-DB and MiBIG making it the best candidate for the biosyntheticSPAdes assembly.

	S. Lividans TK24 CALC	*S. coelicolor* CALC
	DSS	DSS
CALC_1	0.250	0.276
CALC_2	0.253	0.307

Supplementary Table S6. Comparing the DSSs between the two putative BGCs and the two reference BGC from antiSMASH-DB and the reference BGC from MiBIG.

The domain twins generated by the Hungarian algorithm reveal significant differences between the domain structures produced by the rural postman algorithm for the two putative CALC BGCs which affect the order of entire genes within the gene cluster (Supplementary Figure S7).

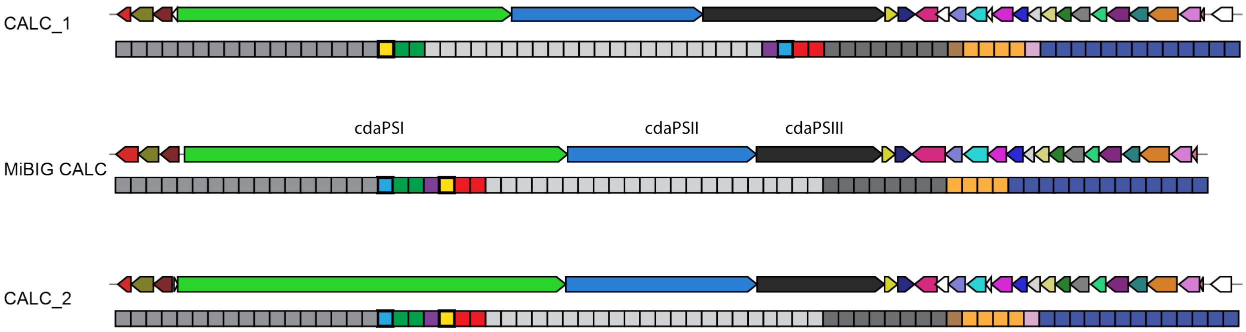

Supplementary Figure S7. The domain orders of CALC_1, CALC_2 and reference CALC from MiBIG. The cdaPSI and cdaPSIII genes from the reference were matched with the green and black labeled genes in CALC_1 and CALC_2. However, the cdaPSI gene in CALC_1 is shorter than the corresponding gene in the reference and in CALC_2, while the cdaPSIII gene (in black) is longer in CALC_1 compared to the reference and CALC_2. These differences are due to an incorrect assembly in CALC_1. This indicates that CALC_2 is the better candidate among the two.

We also assembled the genome of *Streptomyces avermitilis* MA-4680 (Ikegami et al., 2015), which contains a complex repeat-rich gene cluster that produced 6 candidate BGCs from the assembly graph. The ranking algorithm compared the pBGC structures with the filipin BGC, a polyketide synthase BGC, which is present in both antiSMASH-DB and MIBiG (accession: BGC0000059). Supplementary Table S7 illustrates that two out of six candidate BGCs (FILIPIN_2 and FILIPIN_6) produced an identical domain arrangement and the highest-ranking candidate was chosen based on small differences in amino acid sequence.

Putative BGC	**Correctly ordered domain twins**
FILIPIN_2	102/125
FILIPIN_6	102/125
FILIPIN_3	100/125
FILIPIN_1	100/125
FILIPIN_5	100/125
FILIPIN_4	99/125

Supplementary Table S7. Number of domain twins which had the same order between the putative BGC structure and the reference FILIPIN from antismash-db. The highest-ranking putative structures FILIPIN_2 and FILIPIN_6 have identical domain order. The tie is broken by the DSS score, which indicated that FILIPIN 2 putative BGC had higher sequence similarity to the reference.

Supplementary Figure S8 illustrtaes that the domain architecture for candidates 2 and 6 is more similar to the reference BGC domain architecture compared to lower-ranking pBGCs such as candidate FILIPIN_5.

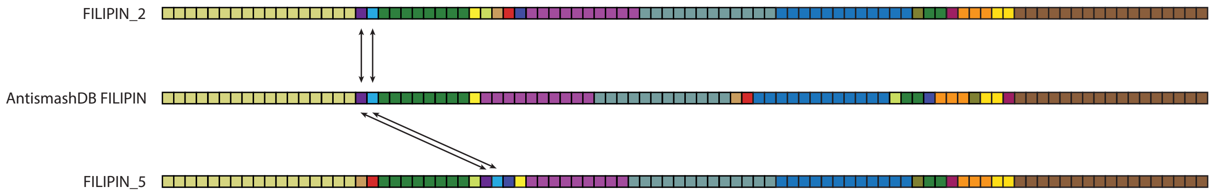

Supplementary Figure S8. The domain orders of two of the FILIPIN putative BGCs and reference FILIPIN from AntismashDB. The domains are color coded to represent blocks with conserved order in the three BGCs even when considering twin domains. The black arrows highlight an example of relocation of two domains for which the reference agrees on the placement for only one of the putative BGCs, notably the highest scoring putative FILIPIN.

As for other reference-based methods, the ranking is affected by database completeness and correctness. Also, the top-ranking pBGC is not necessarily 100% correct, as complex BGCs with high repeat content can result in misassemblies, even with biosyntheticSPAdes. Therefore, results from the ranking algorithm will give insight on which structure better matches the reference BGC but do not guarantee that the highest-ranking structure is also the actual sequence in the assembled genome. In the case of the filipin BGC, even the top-ranking pBGC has small differences with the reference, indicating that further analysis (e.g., by PCR) would be necessary to confirm the actual structure. We provide this example as a case in point to not blindly trust the results of biosyntheticSPAdes and instead verify them whenever possible.

References

Boudreau, P. D., Monroe, E. A., Mehrotra, S., Desfor, S., Korobeynikov, A., Sherman, D. H., ... & Gerwick, W. H. (2015). Expanding the described metabolome of the marine cyanobacterium Moorea producens JHB through orthogonal natural products workflows. *PLoS One*, 10(7), e0133297.

Cummings, S. L., Barbé, D., Leao, T. F., Korobeynikov, A., Engene, N., Glukhov, E., ... & Gerwick, L. (2016). A novel uncultured heterotrophic bacterial associate of the cyanobacterium Moorea producens JHB. *BMC Microbiology*, 16(1), 198.

Kleigrewe, K., Almaliti, J., Tian, I. Y., Kinnel, R. B., Korobeynikov, A., Monroe, E. A., ... & Gerwick, L. (2015). Combining mass spectrometric metabolic profiling with genomic analysis: A powerful approach for discovering natural products from cyanobacteria. *Journal of Natural Products*, *78*(7), 1671-1682.

Kuhn, H. W. (1955). The Hungarian method for the assignment problem. *Naval Research Logistics (NRL)*, *2*(1-2), 83-97.

Mohimani, H., Gurevich, A., Mikheenko, A., Garg, N., Nothias, L. F., Ninomiya, A., ... & Pevzner, P. A. (2017). Dereplication of peptidic natural products through database search of mass spectra. *Nature Chemical Biology*, *13*(1), 30-37.

Wang, M., Carver, J. J., Phelan, V. V., Sanchez, L. M., Garg, N., Peng, Y., ... & Porto, C. (2016). Sharing and community curation of mass spectrometry data with GNPS. *Nature Biotechnology, 34(8)*, 828.

Wick R.R., Schultz M.B., Zobel J. & Holt K.E. (2015). Bandage: interactive visualization of de novo genome assemblies. *Bioinformatics, 31(20),* 3350-3352.